Int. J. Heat Mass Transfer. Vol. 31, No. 6, pp. 1279–1288, 1988
Printed in Great Britain

0017–9310/88 $3.00 + 0.00

Local steady-state natural convection heat transfer in vertical parallel plates with a two-dimensional rectangular rib

Y. H. HUNG and W. M. SHIAU
Department of Power Mechanical Engineering, National Tsing Hua University, Hsinchu, Taiwan 30043, R.O.C.

(*Received* 10 *September* 1987 *and in final form* 16 *November* 1987)

Abstract—Both quantitative measurements and qualitative flow visualization are used to interpret local/average natural convection heat transfer characteristics in vertical parallel plates, with a two-dimensional rectangular rib, under asymmetric isoflux heating. A statistical model of randomized block analysis is introduced to corroborate that the channel spacing varied in the present experiments has no significant effect on average heat transfer characteristics if convective heat flux is maintained constant. Although the range of local modified Rayleigh number studied is in the laminar regime for an equivalently heated flat plate, the heat transfer characteristics in the downstream region of obstruction are much like those in the turbulent regime. Therefore, two new *Nu* correlations for representing local characteristics in the downstream region of the rib and for evaluating average heat transfer performance have been proposed, respectively.

INTRODUCTION AND BACKGROUND

VERTICAL two-dimensional channels formed by parallel plates are a frequently encountered configuration in convection air cooling of electronic equipment, ranging from transformers to main-frame computers and from transistors to power supplies. Packaging constraints and electronic considerations, as well as devices or system operating modes, lead to a wide variety of heat dissipation profiles along the channel walls. In many cases of interest, four kinds of thermal wall conditions (i.e. two symmetric isothermal plates, a single isothermal plate and an insulated plate, two symmetric isoflux plates, and a single isoflux plate and an insulated plate) are proposed to yield approximate conditions in the prediction of the thermal performance of such configurations [1].

Actually, identical flat pack electronic components, mounted on multilayer printed circuit boards (PCBs) with thin copper strips, copper pads or aluminum heat sink plates, are often placed next to one another. When each component dissipates approximately the same amount of power, the heat load will be a uniform isoflux heat profile. If any row of electronic components is considered, the heat dissipation can be evaluated as a uniformly distributed isoflux heating, and this row of electronic components can properly be simulated by a two-dimensional large rib with isoflux heating. Therefore, compared with a smooth isoflux heating plate, a plate mounted with vertically parallel ribs under isoflux heating is more representative of the real geometric configuration and heating condition of PCBs. As we know, the effect of S/B, where S is the streamwise pitch between two adjacent ribs (measured centerline to centerline) and B is the rib height, on flow characteristics and heat transfer performance in such configurations is significantly important. However, natural convection in vertical parallel plates mounted with an array of ribs under isoflux heating is very complicated. Therefore, as a bridge to these kinds of complex problems, it is recognized as useful and valuable to perform a preliminary study of natural convection on a regularly ribbed obstruction mounted on a vertical plate with isoflux heating, especially on the experimental investigation of local steady-state phenomenon.

The investigations about a vertical channel formed by heating plates leaned heavily toward the heat transfer problems of flat plates with different thermal boundary conditions in the past. The most important fundamental studies are those of Aung [2], Aung *et al.* [3], Miyatake and Fujii [4], Miyatake *et al.* [5], and Hung and Perng [6]. These experimental results can be used in the cooling system of electronic equipment. However, there have been relatively few published studies directly related to the natural convective heat transfer in simulating the heat-emitting elements mounted on PCBs. The most representative one was reported by Ortega and Moffat [7]. Results were presented for a series of experiments designed to measure the steady natural convective heat transfer rates and thermal characteristics of a regular array of cubical roughness elements mounted on an insulating plane wall, with and without an opposing insulating wall in that paper. In 1986, Ortega and Moffat [8] dealt with natural convection air cooling of electronic components. Heat-dissipating components are commonly arranged in in-line arrays on a vertical insulated circuit board, facing the back of an adjacent board. The channel thus formed is asymmetrically heated, and the hot surface has large roughness elements. However, no local results were reported in their study.

NOMENCLATURE

B	rib height
C_p	specific heat at constant pressure
g	gravitational acceleration [m s^{-2}]
h	heat transfer coefficient [W m^{-2}°C^{-1}]
H	channel spacing
k	thermal conductivity [W m^{-1}°C^{-1}]
l	rib overall length, defined in Fig. 3
L	channel height, defined in Fig. 3
Nu_L	average Nusselt number, $q_c'' L/k(\overline{T_w - T_0})$
Nu_x	local Nusselt number, $q_c'' X/k(T_w - T_0)$
Q	heat flow rate
q''	heat flux
Ra_L^*	modified Rayleigh number, $C_p\rho^2\beta g q_c'' L^4/\mu k^2$
Ra_x^*	local Rayleigh number, $C_p\rho^2\beta g q_c''(x^*)^4/\mu k^2$
T	temperature
x	coordinate along surfaces of base and rib of test plate, defined in Fig. 3
x^*	axial coordinate along test channel, defined in Fig. 3
X	dimensionless coordinate along surfaces of base and rib of test plate defined in Fig. 3, x/l.

Greek symbols

β	thermal expansion coefficient [K^{-1}]
δ_x	local thermal boundary-layer thickness
μ	dynamic viscosity [kg m^{-1} s^{-1}]
ν	kinematic viscosity, μ/ρ
ρ	density [kg m^{-2}].

Superscript

$\bar{}$	average.

Subscripts

c	convection
i	total
k	conduction
L	based on channel length
r	radiation
w	at test surface
0	at channel inlet or the ambient.

In general, from the foregoing literature survey, information on experimental local steady-state natural convection heat transfer in two vertical parallel plates mounted with a rectangular ribbed obstruction is scarce; and the various factors affecting the local steady-state heat transfer behaviors in this field have not been systematically investigated.

In order to advance our fundamental understanding on local steady-state heat transfer of natural convection in vertical parallel plates mounted with a 2-D rectangular rib under asymmetric isoflux heating, a systematic experiment has been performed. The objectives of this research include: (1) to obtain a systematic experimental data base for the local steady-state natural convection heat transfer behaviors in such a geometric configuration; (2) to observe the effects of channel spacing and wall heating condition on local steady-state heat transfer phenomena through measurements and smoke visualization; (3) to compare the present experimental data with the existing theoretical and experimental results for the cases of vertical smooth plates; (4) to establish a correlation of Nu for the heated plate and rib with a wide range of system parameters such as Grashof number and ratio of channel spacing to rib height; and (5) to propose an effective modelling which can deal with the predictions of the experimental heat losses and local heat transfer performance in the steady-state condition.

EXPERIMENTAL APPARATUS AND PROCEDURES

Figure 1 shows the overall experimental assembly which consists of the entire apparatus and the main instruments. The measurements for the present experiments are performed in a low-turbulent open-loop wind tunnel, which is designed to be used for natural, forced, and mixed convection tests. The wind tunnel facility is in a buoyancy assisting flow condition.

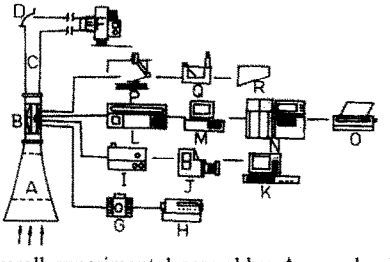

FIG. 1. Overall experimental assembly: A, nozzle; B, test section; C, buffer zone; D, cover plate; E, flexible tube; F, blower; G, transformer; H, digital multimeter; I, smoke generator; J, video camera; K, video recorder and monitor; L, Fluke 2280 B data loger; M, IBM PC-XT computer; N, Apollo computer; O, Epson LQ-2500 printer; P, active Pitot-tube supporter; Q, Dwyer microtector; R, Dwyer air meter.

Wind tunnel facility

A nozzle is made of 2 mm thick steel sheet, and designed to have a contraction in two directions with a 10 : 1 inlet : test-section area ratio. Air enters from the inlet of the nozzle. There are two air-straighteners installed along the nozzle length for adapting the flow and reducing the turbulence level in the test section. The functions of this nozzle are to accelerate the fluid flow and to make a uniform velocity field in forced-convection experiments.

A transparent test section, made of 5 mm thick acrylic-plastic material with a channel of 20 × 40 cm in cross

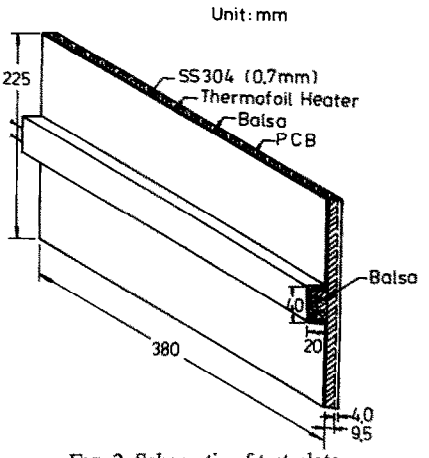

FIG. 2. Schematic of test plate.

section, is designed for the purpose of flow visualization. Two active doors are built in the front as well as at the back of the test section. In addition, an adjustable supporting mechanism is provided in the test section to fix the test plates vertically and horizontally. Small openings on each side of the test section permit passage of thermocouples and electrical wires. Several small holes of 0.16 cm diameter are drilled on the backside acrylic-plastic door of the test section to permit movement of the pitot tube and its support to any designed location within the test section via a self-designed traverse and longitudinal mechanism. During the experiments, all openings and holes are sealed to provide smooth surfaces in the test section.

The buffer zone is located above the test section. There is a 90° bending cover plate on the turn. If natural convection experiments are performed, the cover plate has to be taken away for natural ventilation.

An a.c. variable frequency controller is used to control the blower speed and to adjust the air velocity through the test channel at a specified value. Besides, a flexible plastic tube is installed between the blower and the buffer end of the wind tunnel to abate the influences caused by the vibration of the blower on the test section. To prevent the ambient air in the outside door from flowing back to the test section via the blower and buffer zone so as to affect the natural convection phenomenon, the flexible tube is disconnected and the end of buffer zone sealed prior to the operation of natural convection experiments.

Test plate

The schematic of the overall test plate is shown in Fig. 2. The test plate is 38.0 cm wide and 22.5 cm high. It consists of a 0.07 cm thick stainless steel sheet, two 0.03 cm thick thermofoil heaters, and a composite base plate. A 0.4 cm thick fiberglass board and a 1.0 cm thick balsa plate are epoxied together to form the base board. This board is used to inhibit conductive heat losses from the heaters. The heaters can be applied to a voltage range of 0–140 V with 545 Ω resistance, they are used for heating the stainless steel test surface. The stainless steel test surface is the primary part of the test plate. It is polished to minimize the surface roughness and emissivity, hence radiative heat losses. The emissivity of the test surface is estimated as 0.10 in the present experiments. The SS304 sheet with a dimension of 38.0×26.5 cm and 0.7 mm in thickness is folded into an extruding shape, two 19×26.5 cm thermofoil heaters with a thickness of 0.03 cm are epoxied on its inner surface for heating, and there are 60 calibrated thermocouples for temperature measurements. Finally, the stainless steel test surface with heaters is then epoxied to the composite base board, and another 18 calibrated thermocouples are installed on both sides of the fiberglass board to estimate the conductive heat losses.

Apparatus and instrumentation

As previously described, the test plate has 543 and 548 Ω resistive elements embedded in it for heating, and 78 T-type calibrated thermocouples which are epoxied on the specified locations for temperature measurements. Therefore, the local temperature distribution along the test surface including the extruding element is accurately measured. The air temperatures at the inlet and outlet of the test channel are also measured with two T-type thermocouples, respectively. The temperature difference measured by two thermocouples either at the inlet or outlet is consistently small.

Two 0–140 V transformers supply the power to heaters for making the input power changeable. A GDM-8035F digital multimeter is utilized to calibrate the voltage of each transformer. The channel spacing between the test plate and an adiabatic shrouding plate is measured by a 30 ± 0.05 cm precise ruler. Moreover, both the horizontal and vertical of the test plates are calibrated by the water level.

An NPL-type FVSP 204 smoke generator system is chosen to produce smoke passing the test section for flow visualization. In this system, oil is pumped to the tip of the probe, where an electrical coil heats it to produce a properly dense mist. The probe is shaped to provide a smooth emission of 'smoke' into the surrounding air while minimizing the generation of a wake that could invalidate the flow visualizations.

Data acquisition and control

The experiments are controlled and data acquired automatically with a FLUKE-2280B data logging system interfaced to PC-XT based peripherals. The interface between the computer and the test plate is a 2280 Digital Acquisition and Control Unit. The unit has 160 channels of scannable thermally-compensated relays which are connected to the thermocouples. The data logging system records the local temperature distributions of the test plate during the experiments.

Data reduction

The objective of the data reduction is to calculate the local/average heat transfer coefficients and Nusselt numbers of the test surface. The primary data-reduction program, 'PROLOG', is designed to perform data acquisition, inspection for anomalous behavior, storage, and manipulation. This program can automatically record the measured temperature data on a floppy disk. The other important data-reduction program, 'FINAL', is also developed in PASCAL language to analyze primitive data acquired from 'PROLOG'. The fundamental concept in the 'FINAL' program for steady-state experiments is based on the following equation:

$$Q_c = Q_i - Q_r - Q_k. \quad (1)$$

This energy-balance equation calculates the net convective heat flow rate, Q_c, from the test surface to the air in the test channel. The total power input to the test plate is Q_i and the radiative heat loss from the stainless steel surface to its surroundings is Q_r. It is evaluated using a two-node diffuse gray-body network, with interaction between every side of the element with the base wall and with the shrouding wall [9]. The maximum radiative heat loss is less than 6.55% of the total input power for all cases considered in the present study. The conductive heat loss to the insulated board Q_k is estimated by a subprogram, 'CONDUCTION' in 'FINAL'. The important factors to affect the predictions of these conduction heat losses are the thermal conductivities of the balsa wood and fiberglass board used in the present experiments. Typical thermal conductivities of balsa wood are presented in ref. [10]. In general, the thermal conductivity of balsa wood increases with increasing its density. Thus, with the typical data from ref. [10], the density of balsa wood used in the experiments is measured with a precision balance and the thermal conductivity of balsa wood is determined with an interplating method. Furthermore, in order to obtain the thermal conductivity of fiberglass board, an experiment for measuring the ratio of thermal conductivity of balsa wood to fiberglass board is performed, and the detailed procedure and results are shown in ref. [11]. Other relevant information about the proposed analytical model of the estimation of conductive heat losses to the base board in the present research can also be found in ref. [6].

After Q_r and Q_k are estimated, the net convective heat flow rate from the stainless steel surface, i.e. Q_c can be obtained. Therefore, the local heat transfer coefficients and Nusselt numbers at locations concerned in the steady-state experiments are finally calculated.

Uncertainty analysis

Uncertainty and sensitivity analysis is used extensively in the experimental planning stage to help design the apparatus and data reduction procedures. The method used is the standard single-sample uncertainty analysis proposed by Kline and McClintock [12]. The flow chart for uncertainty analysis and the data-reduction equations for the main measured quantities are shown in ref. [11]. The detailed nominal values of uncertainties about the main contributing variables are tabulated in ref. [11], too. In the experiments, temperature measurements are accurate to within $\pm 0.2^\circ$C, the uncertainty of the power input q_i'' is determined to be 0.25%, and those of Ra and Nu for the ranges of parameters studied in the experiments are within 6.24 and 4.54%, respectively, except for the cases with very small H and q_c'' values.

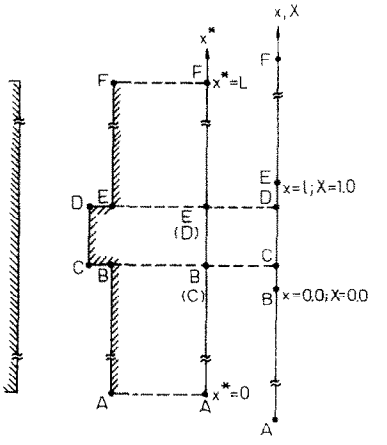

FIG. 3. Coordinate systems for test surface.

EXPERIMENTAL RESULTS AND DISCUSSION

The parameters studied in a series of experiments are channel spacings between 4 and 16 cm (i.e. $H/B = 2$–8), and convective heat fluxes ranged from 41.32 to 269.35 W m^{-2}. Twenty data sets with various channel spacings and convective heat fluxes are presented in the experiments. It is reasonable to consider the cases with $H = 16$ cm (i.e. $H/B = 8$) as the same as the isolated-plate cases in natural convection.

The present results mainly emphasize the local steady-state characteristics. To assist in explaining the distributions of local heat transfer performance, flow visualization is conducted through a smoke generator in the steady state. It must be kept in mind that the case with the dimensionless channel spacing of $H/B = 4.0$ and convective heat flux of $q_c'' = 173.25$ W m^{-2} is chosen as the typical reference in the present experiments.

In order to bring an easy understanding of the results and discussion in this section, the coordinate system used for these kinds of geometric configurations is shown in Fig. 3. In the figure, x^* represents the axial coordinate along the test channel; x represents the coordinate along the surfaces of the base and rib of the test plate; and l is the length of BCDE as shown in the figure.

Before the experimental results of the steady-state condition are displayed, it is necessary to choose the steady state of each experiment. Usually, the steady-

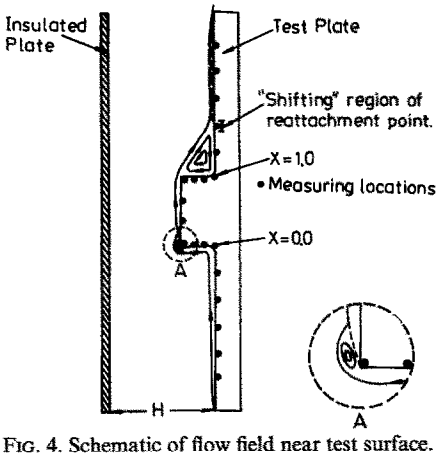

FIG. 4. Schematic of flow field near test surface.

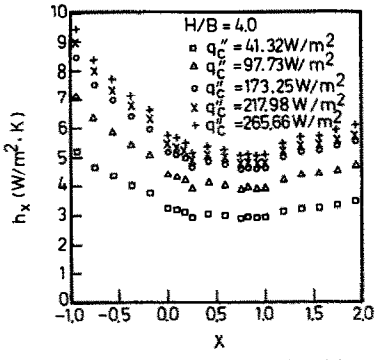

FIG. 5. Effect of convective heat flux on local heat transfer coefficients along test surface.

state condition is considered to be achieved when the q_c'' variation with time is less than 1.0% of the previous q_c'' value in each experiment. In general, the steady-state condition will be achieved about 150–180 min after the power is turned on.

Local heat transfer characteristics

As compared with the local measured temperatures at the center column of the test section, the maximum deviations of the local spanwise temperature measurements in three columns for all experiments are less than 5.6%. Therefore, the two dimensionality of all experimental results is assured in the steady-state period. Figure 4 shows the flow field scheme depicted in aid of the flow visualization through a smoke generator. This figure would be beneficial for analyzing the experimental results. Figure 5 displays the distributions of local heat transfer coefficients under five different heat fluxes with the fixed channel spacing of $H/B = 4.0$. This figure demonstrates that the local heat transfer coefficients increase as the convective heat flux rises. There are two main factors affecting the heat transfer coefficient at each location, i.e. the average thermal conductivity of air in the thermal boundary layer and the thickness of the thermal boundary layer at that location. This can be expressed as

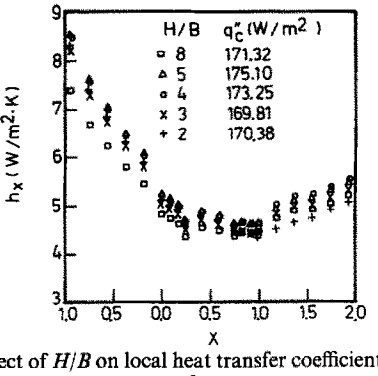

FIG. 6. Effect of H/B on local heat transfer coefficients along test surface.

$$h_x \propto (k/\delta)_x \tag{2}$$

where h_x is the local heat transfer coefficient, k_x the thermal conductivity in the thermal boundary layer at each location x, and δ_x the local thermal boundary layer thickness. As the heat flux increases, the temperature of air adjacent to the heating surface will rise and cause an increase of the thermal conductivity of air near the test surface. Moreover, from the order of magnitude analysis [11], it evidences that the thermal boundary layer will become thinner as the convective heat flux increases. Both effects lead to the increase of the heat transfer coefficient at any specified location x. From this figure, the same tendency of the distribution of local heat transfer coefficients is found for the cases with various convective heat fluxes.

Figure 6 shows the distributions of local heat transfer coefficients for the cases with five different channel spacings at almost the same heat flux. This figure evidences that the channel spacing seems to bring no effect on the local heat transfer coefficients in this range. The verification of this inference can be accomplished by referring to the flow field scheme in Fig. 4. In this scheme, the boundary layer is so thin that even in the experiment with the narrowest channel spacing, i.e. $H = 4.0$ cm or $H/B = 2$, there is still no interaction between the insulated shrouding plate and the boundary layer on the test surface. Therefore, channel spacing has no effect on the local heat transfer coefficients or local Nusselt numbers at a specified location if the heat flux is kept constant in the present experiments. Similarly, the average heat transfer coefficient and average Nusselt number derived from their local values respectively offer the same inference.

Although different heat fluxes will result in different distributions of local heat transfer coefficients as shown in Fig. 5, they all present the same tendency if more careful observations are made on this figure. For convenience, the typical case with channel spacing $H = 8.0$ cm (i.e. $H/B = 4$) and convection heat flux $q_c'' = 173.25$ W m^{-2} is chosen as a representative of all the experiments. The flow visualization depicted in Fig. 4 will contribute to further clarify the experimental results shown in Fig. 6. The coordinates of X varying from 0 to 1.0 represent the extended surface

range of the rib, which is defined in Fig. 3. Three regions had better be presented before interpreting the results, i.e. the region below the rib ($-1.0 < X < 0$), the rib itself ($0 \leqslant X \leqslant 1.0$), and the region above the rib ($1.0 < X < 2.0$). The three regions will be investigated respectively. In addition, four important fundamentals are suggested to demonstrate the results shown in Fig. 5.

(1) With the same heat flux, the thermal resistance will become larger as the boundary layer becomes thicker. It causes the temperature drop between the test surface and the air adjacent to the edge of the thermal boundary layer to rise. It also means a smaller heat transfer coefficient. In brief, a thicker boundary layer means a smaller heat transfer coefficient if the heat flux is kept constant.

(2) The recirculation handicaps heat transfer, i.e. if a recirculation is brought about, the heat transfer coefficients in the backflow region will drop. The layer formed with this recirculation zone is called a 'shear layer' instead of a 'boundary layer'.

(3) For a horizontal plate with the lower surface heated, the induced convection currents are less than those of a heated vertical plate because the horizontal plate tends to block the induced convection currents.

(4) The origin of turbulence depends heavily on the initial disturbance in the flow, and the existence of the turbulence facilitates the heat transfer. It means that if the turbulence gets stronger, the heat transfer coefficient will increase. Having the foundations in the interpretations of these experimental results established, the following paragraphs will present the experimental interpretations.

Region I ($-1.0 < X < 0$): *the region below the rib*

This region is similar to a vertical heated wall. In this region, the boundary layer grows thicker gradually from the leading edge of the test surface to the rib, as can be found in Fig. 4. This phenomenon with the first fundamental mentioned above explains why the local heat transfer coefficients will decrease as the distance from the leading edge is increased. That is, as X increases, the boundary layer thickens, and the local heat transfer coefficient decreases.

Region II ($0 \leqslant X \leqslant 1.0$): *the rib*

This region is divided into three subregions, the first is a short horizontal wall with the lower surface heated ($0 \leqslant X \leqslant 0.25$), the second a heated short vertical wall ($0.25 \leqslant X \leqslant 0.75$), and the third a short horizontal wall with the upper surface heated ($0.75 \leqslant X \leqslant 1.0$). As can be seen in Fig. 6, the local heat transfer coefficients in the first subregion are less than those in Region I. This phenomenon can be interpreted by referring to Fig. 4. The boundary layer formed everywhere in this subregion is thicker than the one formed in Region I. Hence, the first fundamental functions again. As for the thickening of the boundary layer in this subregion, it can be explained by the third fundamental. That is, the induced convection currents are blocked by the horizontal wall. In addition, the reason why the heat transfer coefficient at each location in this subregion will decrease as X increases is that the boundary layer becomes thicker when X gets larger.

In the second subregion, two factors affect the local heat transfer coefficients, that is, the boundary layer extending from the first subregion and the boundary layer re-formed in this subregion. The interactions of these two boundary layers cause a recirculation zone to form and make the outline of the resultant boundary layer look like the shape shown in Fig. 4. From this figure, the connection between the first subregion and the second subregion (i.e. $X = 0.25$) lies in the recirculation zone, and the shear layer formed is thicker than the boundary layers formed in the other three locations measured in this subregion. The boundary layer extended from the first subregion leads to such a peculiar phenomenon. This recirculation hinders the convection currents and leads to the lowest heat transfer coefficient in this subregion. As for the other three locations measured, the boundary layer re-formed in this subregion is dominant. When X is increasing, the re-formed boundary layer becomes thicker. It causes the local heat transfer coefficients measured in these three locations to present a decreasing tendency as X is increasing. Over the second subregion, there exists a sudden expansion. It results in a recirculation zone. Thus, the backflow produced will diminish the induced buoyancy flow and cause the heat transfer coefficient to drop as previously suggested in the second fundamental. This is the reason why the heat transfer coefficients in the third subregion and at location $X = 0.25$ are lower than those at any other measured location on the test surface. In this subregion, the surface is horizontal and the convection currents induced by the buoyancy force are of the same size everywhere. Finally, all the heat transfer coefficients measured in this subregion have about the same value.

Region III ($1.0 < X < 2.0$): *the region above the rib*

Based upon the results of heat transfer measurements with flow visualization in all the experiments, two factors are found to affect the local heat transfer coefficients in this region. That is, the recirculation zone formed by virtue of the existence of the sudden expansion and the turbulence originated near the end of the recirculation zone. The air flow shed from the recirculation zone destroys the boundary layer which should originally be re-formed above the reattachment point. Therefore, the turbulence is produced from the location near the reattachment point. Now look at Figs. 4 and 6, the positions $X = 1.1875$ and 1.375 are located inside the recirculation zone. As the location measured goes farther from the rib, the recirculation becomes weaker and causes the heat transfer coefficient to rise. This explains the tendency of the local heat transfer coefficients in the interval from $X = 1.0$ to 1.375 in Fig. 6.

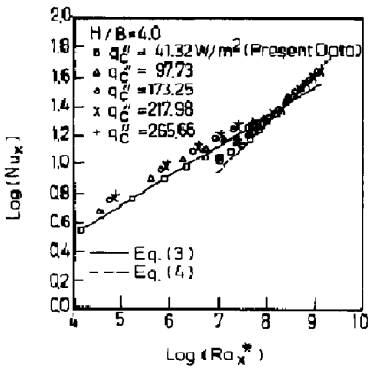

FIG. 7. Relationships between Nu_x and Ra_x^* for cases of $H/B = 4$ with various convective heat fluxes.

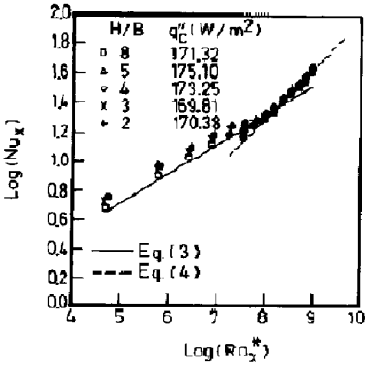

FIG. 8. Relationships between Nu_x and Ra_x^* for cases of $q_c'' = 172$ W m^{-2} under various H/B values.

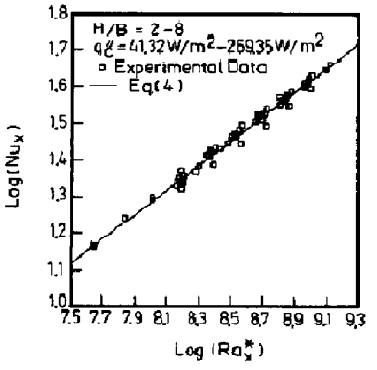

FIG. 9. Relationships between Nu_x and Ra_x^* in the downstream region of the rib.

Before the last three measured locations are discussed, the position of the reattachment point should be pinpointed in advance. From Fig. 6, it can be seen that the reattachment point is 'shifting' in the interval from about $X = 1.33$ to 1.39. Each of the last three locations measured ($X = 1.5625$, 1.75, 1.9375) lies outside the recirculation zone and the turbulence produced will have more effect on the heat transfer coefficients. Thus, as X is farther from the reattachment point, the turbulence becomes stronger and the heat transfer coefficient increases. Another factor influencing the turbulence is the 'sudden expansion' at the outlet of the test plate. As the confined heated wall disappears, the ambient cool air brings destructive effects on the boundary layer near the outlet of the test plate. It strengthens the turbulence and makes the heat transfer coefficients near the outlet increase.

The relationships between Nu_x and Ra_x^* for cases of $H/B = 4$ with various convective heat fluxes are shown in Fig. 7. This figure presents the results that the heat transfer characteristics in the upstream region of the rib are of the laminar-flow type while those in the downstream region of a turbulent-flow type. It can be verified simply by connecting the corresponding experimental results in both regions with a line. Then the slope of the line in each region equals about 1/5 in the upstream region and 1/3 in the downstream region [13]. This confirms the inference made in the region above the rib to a great degree, i.e. turbulence exists in the downstream region of the reattachment point.

Figure 8 shows the relationships between Nu_x and Ra_x^* for the cases of $q_c'' = 172$ W m^{-2} under various H/B values. It offers a conclusion that the channel spacing has no significant effect on the experimental results based on different channel spacings in the present experimental range, i.e. $H/B = 2.0$–8.0. It also presents the results that the heat transfer in the upstream region of the rib is of laminar type and of turbulent type in the downstream region as mentioned previously in Fig. 7. To predict the local Nusselt number at any location on the test surface with a known convective heat flux, the correlation equation (3), which can be found in refs. [15, 16], and a new proposed asymptotic limit, i.e. equation (4), acquired by collecting all the experimental data about the local Nusselt numbers in the downstream region of the rib, are presented in the following:

$$Nu_x = 0.519 Ra_x^{1/5} \quad \text{if } X \leqslant 0.75 \tag{3}$$

$$Nu_x = 0.252 Ra_x^{1/3} \quad \text{if } X > 0.75. \tag{4}$$

The experimental data for the cases with $H/B = 2$–8 and $q_c'' = 41.32$–269.35 W m^{-2} at $X > 0.75$ are depicted in Fig. 9, equation (4) is also plotted in this figure with a solid line. Similarly, equations (3) and (4) are plotted in Figs. 7 and 8 for comparison with experimental results.

Average heat transfer performances

The average heat transfer coefficients with different experimental conditions are presented in Table 1. Two kinds of effects are contemplated: those of the treatments, which are of major interest to the experiments, and those of the blocks, the contributions of which we desire to eliminate. In practice, blocks have different convective heat fluxes, and treatments are varied channel spacings in the present experiments. The randomized block analysis suggested by Box *et al.* [14] is useful to check whether channel spacing has effects on the average heat transfer coefficients. The analysis

Table 1. Experimental results of average heat transfer coefficients

q_c'' (W m^{-2})	Treatment H/B 2	3	4	8	Block average
42.44	3.81	3.77	3.59	3.73	3.725
97.20	4.71	4.84	5.03	4.73	4.828
170.52	5.49	5.53	5.61	5.31	5.484
217.86	5.97	5.92	6.00	6.08	5.991
266.81	6.25	6.28	6.35	6.27	6.288
Treatment average	5.246	5.268	5.314	5.224	5.263

of the variance table is described in the following paragraphs.

Table 1 summarizes the average heat transfer coefficients with different experimental conditions. In the table, the treatments are $H/B = 2, 3, 4, 8$; and blocks are $q_c'' = 42.44, 97.20, 170.52, 217.86, 266.81$ W m^{-2}.

An observation made with the tth treatment applied to the ith block will be denoted by y_{ti}, the ith block average by $\bar{y}_i$, the tth treatment average by $\bar{y}_t$, and the grand average by $\bar{y}$. Now consider a mathematical model that might describe such a set of data. The simplest model supposes that an observation y_{ti} can be represented as the sum of a general mean η, a block effect β_i, a treatment effect τ_t, and an error ε_{ti}; that is

$$y_{ti} = \eta + \beta_i + \tau_t + \varepsilon_{ti}. \quad (5)$$

Associated with such a model is the decomposition of the observations

$$y_{ti} = \bar{y} + (\bar{y}_i - \bar{y}) + (\bar{y}_t - \bar{y}) + (y_{ti} - \bar{y}_i - \bar{y}_t + \bar{y}). \quad (6)$$

The last quantity of $(y_{ti} - \bar{y}_i - \bar{y}_t + \bar{y})$ is called the residual because it represents what is left after the grand average, block differences, and treatment differences have all been allowed for.

In vector notation the decomposition can be written as

$$Y = A + B + T + R. \quad (7)$$

In this equation each of the symbols Y, A, B, T, and R represents a vector containing $N = nk$ elements. Here n is the number of blocks and k the number of treatments. The 'sum of squares' are sums of squares of the elements and represent the squared lengths of the vectors Y, A, B, T, and R. The general formulas for the sum of squares are given in Table 2. In this table, the number of degrees of freedom is the number of dimensions in which each vector is free to move and is equal to the number of elements that can be selected arbitrarily.

In the present experiment, $n = 5$ and $k = 4$; $S_A = 553.983$, $S_B = 16.736$, $S_T = 0.02218$, $S_R = 0.13547$, $S = 570.877$; the mean squares are $S_B^2 = 138.496$, $S_T^2 = 0.007393$, $S_R^2 = 0.011289$. Compared with the F distribution in ref. [14], the ratios of mean squares are: (1) $S_B^2/S_R^2 = 12268.045 \gg F_{4,12}$ (upper 0.1% points) = 9.63, i.e. it manifests that the effect of the convective heat flux is significant; (2) $S_T^2/S_R^2 = 0.65489 < F_{3,12}$ (upper 25% points) = 1.56, i.e. it evidences that the channel spacing effect is insignificant in the present experiments.

From the above analysis, a conclusion is achieved that the channel spacing has no significant effect on average heat transfer coefficients if the convective heat flux is kept constant. Another conclusion is that the convective heat flux strongly influences the average heat transfer coefficients. Table 1 also carries the message that as the convective heat flux increases, the average heat transfer coefficient rises. Table 3 lists the average Nusselt numbers with different experimental conditions. It presents a similar conclusion as Table 1 does because they both introduce the same tendency.

Figure 10 shows the relationships between the average Nusselt numbers and the modified Rayleigh numbers for all experimental results. The figure manifests that the $\overline{Nu}_L$ correlation, which is derived from equation (3), is applicable only in the experiments with low convective heat fluxes (e.g. $Ra_L^* < 10^8$). This correlation can be expressed as

$$\overline{Nu}_L = 0.649 Ra_L^{*1/5}. \quad (8)$$

As the convective heat flux increases, the turbulence originated in the downstream region of the rib becomes stronger. Thus, a new asymptotic limit with a 0.316 power dependence (a value between 1/5 and 1/3) of the average Nusselt number on the modified Rayleigh number is proposed as follows:

$$\overline{Nu}_L = 0.0617 Ra_L^{*0.316}. \quad (9)$$

Both correlations are plotted in Fig. 10 for comparisons with experimental results. All thermophysical properties appearing in Nu and Ra are evaluated at the film temperature, i.e. $0.5(\bar{T}_w + T_0)$. In the experimental Ra_L^* ranges between 3.75×10^8 and 1.93×10^9, the average deviation of the predictions by equation (8) compared to the present experimental data is 7.45% with a maximum deviation of 11.59%; while the average deviation of the predictions by equation (9) from the experimental data is 1.20% with a maximum deviation of 3.43%.

CONCLUSIONS

Based on the results presented and discussed in the discussion section, the main conclusions are given below.

Table 2. Algebraic decomposition of sums of squares for the randomized block design, general formulas

Source of variation	Sum of squares	Degrees of freedom
Average (correction factor)	$S_A = nky$	1
Between blocks	$S_B = k\sum_{i}^{n}(\bar{y}_i - \bar{y})^2$	$n-1$
Between treatments	$S_T = n\sum_{t}^{k}(\bar{y}_t - \bar{y})^2$	$k-1$
Residuals	$S_R = \sum_{i}^{n}\sum_{t}^{k}(y_{it} - \bar{y}_i - \bar{y}_t + \bar{y})^2$	$(n-1)(k-1)$
Total	$S = \sum_{t}^{k}\sum_{i}^{n} y_{it}^2$	$N = nk$

Table 3. Experimental results of average Nusselt numbers

	Treatment H/B				
q_c'' (W m^{-2})	2	3	4	8	Block average
42.44	32.99	32.67	30.73	31.98	32.091
97.20	40.29	41.03	42.68	40.02	41.005
170.52	46.21	45.88	46.90	44.07	45.763
217.86	49.88	48.84	49.90	49.75	49.595
266.81	51.64	51.37	51.99	50.88	51.469
Treatment average	44.200	43.958	44.439	43.341	43.985

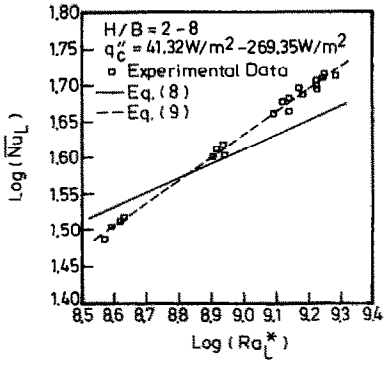

FIG. 10. Relationships between $\overline{Nu}_L$ and Ra_L^* in the experiments.

(1) A systematic experimental data base for the local steady-state natural convection heat transfer in such geometric configurations has been established.

(2) Qualitatively, from flow visualization, the existence of a protruding rib changes the flow characteristics and originates the recirculation zone as well as the turbulence zone in the downstream region of the rib. A reattachment point lies in between both zones.

(3) Through flow visualization and experimental measurements, even in the experiments with the narrowest channel spacing, i.e. $H = 4.0$ cm or $H/B = 2$, the boundary layer produced along the test surface is so thin that there is no interaction between the insulated shrouding plate and the boundary layer. Therefore, the channel spacings studied in the present experiments have no effect on heat transfer behaviors.

(4) In the ranges of parameters studied, a randomized block statistical analysis verifies that channel spacing has no effect while surface heat flux has significant effects on average heat transfer performance in the steady-state condition.

(5) The heat transfer coefficients in the recirculation zone are lower than those in any other region. On the contrary, turbulence profits heat transfer behaviors.

(6) The heat transfer characteristics in the upstream region of the protruding rib behave like laminar natural convection of a vertical flat plate with isoflux heating, while those in the downstream region of the protruding rib reveal a turbulent type. A new asymptotic limit with a 1/3 power dependence of local Nusselt number on local modified Rayleigh number, instead of a 1/5 power dependence for vertical isoflux heating plates, is proposed by a curve-fitting method. This correlating equation is applicable in the downstream region of the rib.

(7) Average Nusselt numbers in the present experiments correlate well with a new asymptotic limit with a 0.316 power dependence on modified Rayleigh numbers based on the channel height.

REFERENCES

1. A. Bar-Cohen and W. M. Rohsenow, Thermally optimum spacing of vertical, natural convection cooled, parallel plates, *J. Heat Transfer* **106**, 116–123 (1984).
2. W. Aung, Fully developed laminar free convection

between vertical plates—heated asymmetrically, *Int. J. Heat Mass Transfer* **15**, 1577–1580 (1972).
3. W. Aung, L. S. Fletcher and V. Sernas, Developing laminar free convection between vertical flat plates with asymmetric heating, *Int. J. Heat Mass Transfer* **15**, 2293–2308 (1972).
4. O. Miyatake and T. Fujii, Natural convective heat transfer between vertical parallel plates at unequal uniform temperatures, *Heat Transfer—Jap. Res.* **2**(4), 79–88 (1973).
5. O. Miyatake, T. Fujii, M. Fujii and H. Tanaka, Natural convective heat transfer between vertical parallel plates with unequal heat fluxes, *Heat Transfer—Jap. Res.* **3**(3), 29–33 (1974).
6. Y. H. Hung and S. W. Perng, An experimental study of local steady-state natural convection in a vertical channel heated on one side wall, accepted by the 25th ASME National Heat Transfer Conference, Houston, Texas, 24–27 July (1988).
7. A. Ortega and R. J. Moffat, Heat transfer from an array of simulated electronic components: experimental results for free convection with and without a shrouding wall, 23rd ASME National Heat Transfer Conference, Denver, Colorado, pp. 5–15, 4–7 August (1985).
8. A. Ortega and R. J. Moffat, Experiments on buoyancy-induced convection heat transfer from an array of cubical elements on a vertical channel wall, HMT-38, Thermosciences Division, Department of Mechanical Engineering, Stanford University, California (1986).
9. R. Siegel and J. R. Howell, *Thermal Radiation Heat Transfer*, 2nd Edn. McGraw-Hill, New York (1980).
10. L. S. Marks, *Mechanical Engineers' Handbooks*, p. 368. McGraw-Hill, New York (1951).
11. W. M. Shiau, Transient/steady-state experiments of natural convection heat transfer in vertical parallel plates with a two-dimensional rectangular rib, Master's Thesis, National Tsing Hua University, Taiwan (1987).
12. S. J. Kline and F. A. McClintock, Describing uncertainties in single-sample experiments, *Mech. Engng* 3, January (1953).
13. S. W. Churchill and H. Ozoe, A correlation for laminar free convection from a vertical plate, *J. Heat Transfer* **95**, 540–541 (1973).
14. E. P. Box, W. G. Hunter and J. S. Hunter, *Statistics for Experimenters*, pp. 208–218, 636–640. Wiley, New York (1978).
15. W. M. Kays and M. E. Crawford, *Convective Heat Transfer*, 2nd Edn, p. 320. McGraw-Hill, New York (1980).
16. E. M. Sparrow and J. L. Gregg, Laminar free flow convection from a vertical plate with uniform surface heat flux, *J. Heat Transfer* **78**, 435–440 (1956).

CONVECTION THERMIQUE NATURELLE LOCALE, PERMANENTE, ENTRE DES PLAQUES PARALLELES VERTICALES AYANT DES BANDES RECTANGULAIRES BIDIMENSIONNELLES

Résumé—Des mesures quantitatives et une visualisation qualitative d'écoulement sont affectuées pour interpréter les caractéristiques locales ou globales de la convection thermique naturelle, entre des plaques parallèles, avec des bandes rectangulaires bidimensionnelles, pour un chauffage asymétrique isoflux. Un modèle statistique d'analyse par bloc est introduit pour corroborer le fait que l'espacement du canal variable dans les présentes expériences n'a pas d'effet significatif sur les catactéristiques thermiques moyennes si le flux convectif est maintenu constant. Bien que le domaine du nombre de Rayleigh modifié, local, est dans le régime laminaire pour une plaque plane chauffée de façon équivalente, les caractéristiques du transfert thermique dans la région d'obstruction sont plutôt semblables au cas du régime turbulent. On propose deux nouvelles formules pour *Nu*, de façon à représenter les caractéristiques locales au voisinage de la bande et pour le transfert global.

ÖRTLICHER WÄRMEÜBERGANG BEI STATIONÄRER NATÜRLICHER KONVEKTION ZWISCHEN SENKRECHTEN PARALLELEN, MIT JE EINER ZWEIDIMENSIONALEN RECHTECK-RIPPE BESETZTEN PLATTEN

Zusammenfassung—Der örtliche und mittlere Wärmeübergang bei natürlicher Konvektion zwischen senkrechten parallelen Platten, welche jeweils eine zweidimensionale Rechteck-Rippe tragen, wurde für den Fall einer asymmetrischen Beheizung mit konstanter Wärmestromdichte mittels quantitativer Messungen und qualitativer Strömungsbeobachtungen untersucht. Mit Hilfe eines statistischen Verfahrens wurde bestätigt, daß der in den Versuchen variierte Kanalabstand keinen erkennbaren Einfluß auf den mittleren Wärmeübergang hat, wenn die Wärmestromdichte konstant gehalten wird. Obwohl die modifizierte Rayleigh-Zahl im laminaren Bereich für eine äquivalent beheizte ebene Platte lag, zeigte der Wärmeübergang stromab vom Hindernis turbulentes Verhalten. Deshalb werden zwei neue *Nu*-Korrelationen für den örtlichen und den mittleren Wärmeübergang stromab der Rippe vorgeschlagen.

ЛОКАЛЬНЫЙ СТАЦИОНАРНЫЙ ЕСТЕСТВЕННО-КОНВЕКТИВНЫЙ ТЕПЛОПЕРЕНОС В ВЕРТИКАЛЬНЫЙ ПАРАЛЛЕЛЬНЫХ ПЛАСТИНАХ С ДВУМЕРНЫМ ПРЯМОУГОЛЬНЫМ РЕБРОМ

Аннотация—Используются как количественные измерения, так и качественная визуализация течения для описания характеристик местного/среднего естественно-конвективного теплопереноса в вертикальных параллельных пластинах с двумерным прямоугольным ребром в условиях асимметричного равномерного нагрева. С помощью статистической модели показано, что расстояние между каналами, изменяющееся в настоящих опытах, не оказывает существенного влияния на средние характеристики теплопереноса, если конвективный тепловой поток поддерживается постоянным. Хотя исследуемый диапазон местного модифицированного числа Рэлея соответствует ламинарному режиму для эквивалентной нагреваемой плоской пластины, характеристики теплопереноса в области вниз по потоку за препятствием очень схожи с характеристиками турбулентного режима. Поэтому предложены два новых соотношения для числа *Nu*, описывающие локальные характеристики ребра в области вниз по потоку и оценивающие осредненный теплообмен.